ACUSTICA · acta acustica
Vol. 84 (1998) 1014 – 1024

Theory and Preliminary Measurements of the Rayleigh-Like Collapse of a Conical Bubble

T. G. Leighton, A. D. Phelps, B. T. Cox, W. L. Ho
Institute of Sound and Vibration Research, University of Southampton, Southampton SO17 IBJ, UK

Summary
Key to the dynamics of the type of bubble collapse which is associated with such phenomena as sonoluminesence, and the emission of strong rebound pressures into the liquid, is the role of the liquid inertia. Following the initial formulation of the collapse of an empty spherical cavity, such collapses have been termed 'Rayleigh-like', and today this type of cavitation is termed 'inertial', reflecting the dominant role of the liquid inertia in the early stages of the collapse. Whilst the inertia in models where, at these early stages, spherical symmetry can be assumed can depend primarily on the liquid density, experimental control of the liquid inertia has not readily been achievable without changing the liquid density, and consequently changing other liquid properties. In this text, novel experimental apparatus is described whereby the inertia at the early stages of the collapse of a conical bubble can easily be controlled. The collapse is capable of producing sonoluminescence. The similarity between the collapse of spherical and conical bubbles is investigated analytically, and compared with experimental measurements of the pressures generated by the collapse.

PACS no. 43.35.Ei, 43.30.Nb, 43.25.Yw

1. Introduction

Eighty years ago Rayleigh [1] published his pioneering analysis for the collapse of an empty spherical cavity under a static pressure. Coupling this energetic collapse phase with the explosive growth phase of a sufficiently small bubble (as expounded by Blake, [2]) to a maximum size $R_{\max}$, Noltingk and Neppiras [3, 4] characterised a particular type of cavitation. In this, appropriately small bubbles in sufficiently strong sound fields undergo growth to many times their original size, and then subsequent rapid collapse. The growth phase is to a first approximation isothermal, and the collapse phase adiabatic, such that the bubble serves to concentrate the acoustic energy. Flynn [5] further distinguished this socalled 'transient' (or 'unstable') cavitation from the less energetic 'stable' cavitation, where the bubble pulsates about an equilibrium radius over many acoustic cycles. Flynn [6] then analysed the energetics of transient collapse, through consideration of the mechanical work done on the cavity by the spherical convergence of the liquid, and the dissipation of energy during the collapse process. An important feature of high-energy cavitation was found to be the dominance of inertial forces during the collapse, and this was taken for many years to be the best definition available for transient cavitation. However there was never an unequivocal basis for ascribing such an energy concentration to the classical interpretation of the phenomenon of 'transient cavitation', which involves sudden growth followed by rapid collapse and rebound, after which the bubble fragments. Nevertheless such collapses were *experimentally* associated with sonoluminescence and spherical shock waves emitted by the rebounding bubble, and occurred in regimes (acoustic pressure, frequency, initial bubble size) where the theories predicted the dominance of inertial forces. The overwhelming evidence was such that in 1985 Roy *et al.* concluded that "if one desires a threshold for 'violent' cavitation, then sonoluminescence is a fitting criterion since the violence of a transient collapse is linked primarily to $R_{\max}$, which corresponds to the energy stored in the liquid" [7], and that "light emission may serve as an ideal indicator of what Apfel [8] calls the 'threshold for transient-violent cavitation' ".

Then in 1990 Gaitan and Crum [9] observed sonoluminescence over measurement intervals of thousands of acoustic cycles from stable cavitation of a single bubble which did not break up, and which exhibited no detecable surface wave or streamer activity. Clearly such bubbles cannot be described as 'transient'. The term 'inertial cavitation' was introduced to indicate those collapses in which the inertial forces dominate, and which consequently would be expected to generate energetic effects such as sonoluminescence: if the bubble performs this once or a few times and then fragments on rebound, the event is what was understood to be tansient cavitation; if the bubble repeats the collapse intact over a great number of cycles, then sonoluminescence from stable cavitation has been achieved.

Whilst the questions of nomenclature raised by the discovery of sonoluminescence from stable cavitation could be fairly readily resolved, those relating to the origin of sonoluminescence could not. Specifically, what is the mechanism by which sonoluminescence is produced; and does it differ when single bubbles undergo stable cavitation from when multiple bubbles undergo inertial cavitation and, as a result of surface instabilities, break up [10, 11, 12, 13]? These will not be discussed here, beyond saying that theories of such origins have historically fallen (though not exclusively) into three main categories [14]: thermal, mechanochemical, and electrical. However the discovery that sonoluminescent light pulses from stable cavitation are less than 50 ps duration with the 'jitter' in time between flashes to be much less than 50 ps, led Barber *et al.* [15] to speculate on the nature of a cooperative/coherent optical (or fluid) phenomenon involved

Received 9 June 1997,
accepted 3 March 1998.

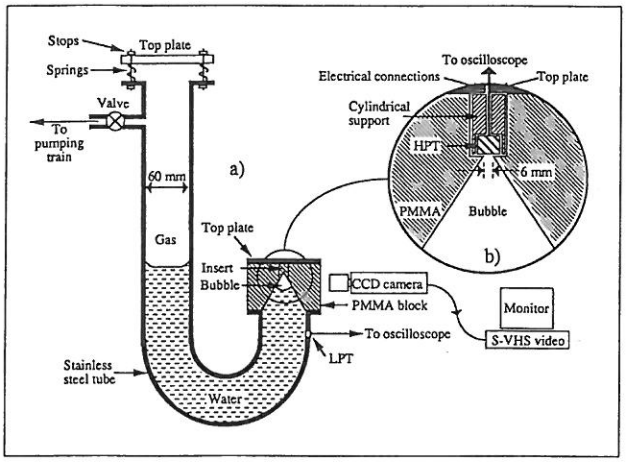

Figure 1. (a) Diagram of the apparatus, showing the positions of the pressure transducers, LPT and HPT; (b) insert showing the detail of the cone tip.

in the mechanism. The discovery stimulated further discussion as to the possible mechanism. Crum and Putterman [16] stated that "As the phenomenon may be too fast for the establishment of local thermal equilibrium, we may be facing a situation where focusing acoustic stress fields are transduced directly into quantum excitations". In this decade there have been publications on how such brief light emissions can be consistent with a range of simulations [17] and theories, including gas shocks [18], rectified diffusion [19], electrical discharge [20], quantum radiation [21], and jetting [22].

Key parameters which feature within these theories include the inertia of the liquid, and the motion and stability/instability of the gas–liquid interface. During inertial cavitation these are not normally accessible to control, or (in the case of details of the bubble wall) measure. In this paper, apparatus enabling more ready access to these parameters is introduced. A gas pocket collapses into an otherwise liquid-filled conical hollow. The cone has a circular horizontal cross-section, which at its base sits on top of a liquid-filled tube of the same diameter. As the bubble collapses, liquid can flow from the tube into the cone (Figure 1). The actual apparatus is shown in Figure 1a, where it can be seen that the tube is in fact fashioned into a U-tube. This allows the following experimental protocol. At equilibrium, under 1 atmosphere, the gas pocket occupies the upper few millimetres of the cone. When the static pressure in the tube is reduced (through closure of the top-plate and application of the pumping train indicated in Figure 1a), the bubble undergoes relatively slow growth. Then the top-plate is opened, and a pressure step of approximately 1 bar propagates down the U-tube, causing the collapse of the bubble. The collapse is specifically designed to be unstable, so that the bubble can be ensured to have undergone fragmentation after the first rebound. The geometry of the bubble is such that it collapses into the solid angle conical section (30° half-angle) of a sphere. This not only allows the imaging of a 'cross-section' of the luminescing bubble, but also allows the positioning of pressure transducers within the gas and within the surrounding liquid, since the centre of the collapse is well-defined. However the liquid surrounding the bubble does not continue in a conical geometry indefinitely, but instead becomes one-dimensional, allowing ready control of the inertia.

1.1. Theory

The basic considerations employed in later formulations of the dynamics of the inertial collapse can be found in the pioneering paper of Rayleigh [1], who considered the collapse of an empty cavity which remains spherical at all times, located in an incompressible liquid. The empty cavity, at rest, is envisaged to be "as if a spherical portion of the fluid is suddenly annihilated", to quote Besant [23]. The cavity at this time, when the wall velocity is zero, is assumed to have a radius R_m. Since the cavity contains no gas, the liquid pressure p_L just outside the cavity is zero (if surface tension is assumed to be negligible). Thus the work done by the hydrostatic pressure p_∞ from that time until the cavity has contracted to a radius R, which is given by $4\pi p_\infty (R_m^3 - R^3)/3$, will simply equal the kinetic energy of the liquid. This is found by integrating the energy over spherical shells of liquid, of speed $\dot{r}$, thickness Δr, and mass $4\pi r^2 \rho \Delta r$, where ρ is the liquid density. Equating the work done to the kinetic energy in this way gives

$$\frac{4\pi}{3} p_\infty (R_m^3 - R^3) = \frac{1}{2} \int_R^\infty \dot{r}^2 \rho 4\pi r^2 \, \mathrm{d}r. \qquad (1)$$

If the liquid is taken to be incompressible, then at a given instant the rate of mass of liquid flowing through any spherical surface (radius r) equicentric with the bubble must be a constant. In time Δt a mass of liquid $4\pi r^2 \rho \dot{r} \Delta t$ flows across a surface at some general radius r outside the bubble. Equating this to the flow at the bubble wall gives

$$\dot{r}/\dot{R} = R^2/r^2. \qquad (2)$$

By substituting equation (2) into (1), integration yields the kinetic energy to be $2\pi\rho\dot{R}R^3$, giving:

$$\dot{R}^2 = \frac{2p_\infty}{3\rho} \left(\frac{R_m^3}{R^3} - 1 \right). \qquad (3)$$

To find the wall velocity, $\dot{R}$, the negative root of equation (3) is taken since, because the wall motion is inwards, $\dot{R}$ must be negative. Integration of equation (3) with respect to time gives the collapse time t_{Ray} of the cavity:

$$t_{\mathrm{Ray}} = \int_{R_m}^{R=0} \frac{\mathrm{d}R}{\dot{R}} \approx 0.915 R_m \sqrt{\frac{\rho}{p_\infty}}. \qquad (4)$$

The assumption that the liquid is incompressible means that the derivation becomes invalid once the velocity of the cavity wall approaches the speed of sound in the liquid. From equation (3) it can be seen that this will always occur at some point during the collapse of an empty spherical cavity. Therefore Rayleigh suggested the presence of some permanent gas within the cavity.

ACUSTICA · acta acustica
Vol. 84 (1998)

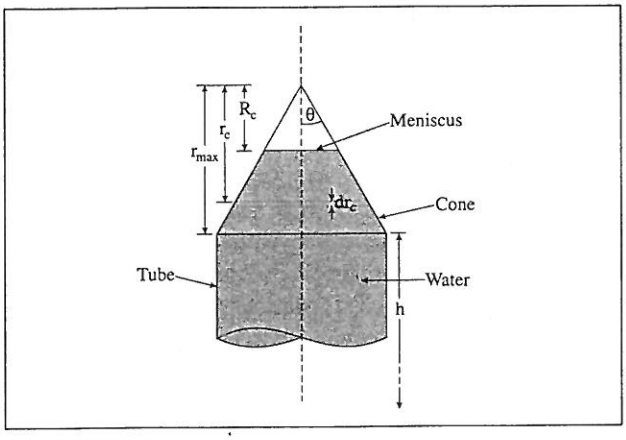

Figure 2. Schematic diagram of the cone and tube, defining the various model parameters.

Clearly there are key differences between the so-called "Rayleigh" collapse, and the collapse considered in this paper. Contrary to what might be supposed, the main difference arises not through the geometry of the cone, but through that of the tube, as the following analysis shows. The layout of the cone and tube is shown schematically in Figure 2, with a definition of the various model parameters. It should be noted in the figure that the section of gas considered has a flat base. When the geometry of the collapses was observed experimentally, it appeared that the meniscus was flat over the majority of the collapse: it was not until the bubble was very small in the tip of the cone, that the meniscus adopted a curved section. Therefore the gas in the apparatus does not exactly represent the collapse of a solid angle section of a spherical bubble. In the following derivation of the equations of motion of the collapse, the meniscus is considered to be flat throughout, because even at the smallest radii the bubble is expected to achieve, the contribution to the internal gas pressure due to the surface tension forces is negligible. Adapting the calculation for a curved meniscus throughout is not difficult, but less relevant to the initial conditions.

Since the cross-sectional area in the cone increases with distance from the meniscus, the flow velocity of the incompressible liquid decreases in proportion. The parameter R_c is the vertical distance from the cone apex to the meniscus (which, neglecting edge-effects, therefore has area $\pi R_c^2 \tan^2\theta$), and r_c is the distance from the cone apex to a circular element of liquid in the cone (of area $\pi r_c^2 \tan^2\theta$). If the liquid is incompressible, then the volume of liquid crossing all such areas in a time $\mathrm{d}t$ must be constant. Equating liquid fluxes gives:

$$\dot{R}_c \mathrm{d}t \pi R_c^2 \tan^2\theta = \dot{r}_c \mathrm{d}t \pi r_c^2 \tan^2\theta \quad \Rightarrow \quad \dot{r}_c/\dot{R}_c = R_c^2/r_c^2. \tag{5}$$

Equation (5) has the same form as equation (2), showing that with respect to the inertia of an incompressible fluid, the cone precisely models a section of spherical geometry. This identity of geometric divergence however does not hold for the fluid in the U-tube. Here there is no divrgence and, to a first approximation, every element of fluid within the tube accelerates to exactly the same degree as the fluid at the base of the cone (if the fluid is assumed to be incompressible). Therefore at the start of the collapse, when the bubble almost fills the cone, the inertia of the liquid is very great. In the conditions pertaining to the start of this experiment therefore, when a pressure step of around one atmosphere is applied to the end of the liquid column remote from the bubble, inertial forces will clearly dominate pressure forces and an inertial collapse will be achievd.

The kinetic energies of the liquid in the cone and the column can be calculated for a given meniscus position R_c. The vertical distance from the apex to the base of the cone (where the cross-sectional area is A_0 and the liquid velocity is $\dot{\varepsilon}$) is $r_{\max}$. Following the arguments that gave equation (5), the liquid velocity a distance r_c below the cone apex is $\dot{r}_c = \dot{\varepsilon} r_{\max}^2/r_c^2$.

The volume of the liquid element there, of thickness $\mathrm{d}r_c$, is $\pi(r_c \tan\theta)^2 \mathrm{d}r_c$; its mass is $\rho\pi(r_c\tan\theta)^2\mathrm{d}r_c$; and its kinetic energy is therefore $\frac{1}{2}\rho\pi(r_c\tan\theta)^2\mathrm{d}r_c(\dot{\varepsilon}r_{\max}^2/r_c^2)^2$. Summing these fluid elements gives the total kinetic energy of the liquid in the cone as

$$\begin{aligned}\Phi_{KE,c} &= \int_{R_c}^{r_{\max}} \frac{1}{2}\rho\pi\left(r_c\tan\theta\right)^2\left(\frac{\dot{\varepsilon}r_{\max}^2}{r_c^2}\right)^2 \mathrm{d}r_c \\ &= \frac{1}{2}\rho\pi\tan^2\theta\, r_{\max}^4\dot{\varepsilon}^2\int_{R_c}^{r_{\max}}\frac{\mathrm{d}r_c}{r_c^2} \\ &= \frac{1}{2}\rho\pi\tan^2\theta\, r_{\max}^4\dot{\varepsilon}^2\left(\frac{1}{R_c}-\frac{1}{r_{\max}}\right).\end{aligned} \tag{6}$$

All elements of the incompressible liquid column (of length h) in the tube will have velocity of $\dot{\varepsilon}$ so that the kinetic energy of the liquid in the tube is

$$\Phi_{KE,t} = A_0\rho h\dot{\varepsilon}^2/2. \tag{7}$$

Clearly h is dependent on R_c, since the liquid components within the tube and the cone must always sum to equal V_l, the total volume of liquid in the apparatus as:

$$\begin{aligned} V_l &= \frac{\pi}{3}\tan^2\theta\left(r_{\max}^3 - R_c^3\right) + A_0 h \\ \Rightarrow \quad A_0 h &= A_0 h_i - \frac{\pi}{3}\tan^2\theta\left(R_i^3 - R_c^3\right),\end{aligned} \tag{8}$$

where h_i is the initial length of water in the tube alone, and R_i is the starting vertical position of the meniscus before plate opening. It may be noted that the effective inertias of the liquid in the column and the cone are equal when the meniscus position is $R_c = R_e$ such that

$$\begin{aligned}&\Phi_{KE,t} = \Phi_{KE,c} \quad \Rightarrow \\ &\frac{1}{2}A_0\rho h\dot{\varepsilon}^2 = \frac{1}{2}\rho\pi\tan^2\theta\, r_{\max}^4\dot{\varepsilon}^2\left(\frac{1}{R_e}-\frac{1}{r_{\max}}\right) \\ &\qquad\qquad \Rightarrow \quad R_e = \frac{r_{\max}^2}{h + r_{\max}}.\end{aligned} \tag{9}$$

Usually the length of liquid in the column at the end of the collapse is about 2 cm shorter than its initial value, so treating the parameter h as approximately constant and substituting

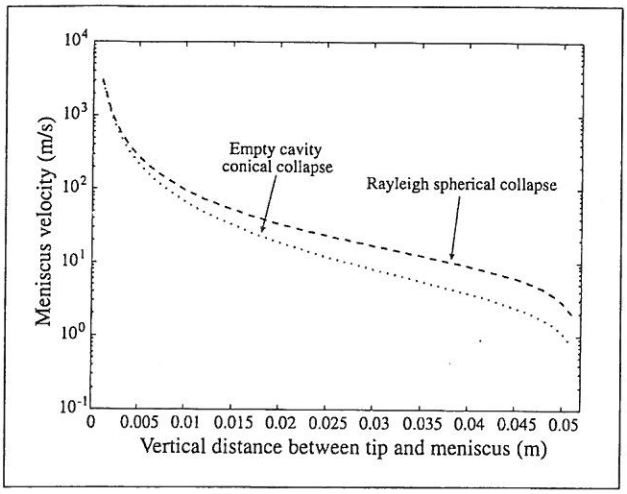

Figure 3. Plot of meniscus velocity against: bubble radius for the Rayleigh collapse of a spherical, empty bubble (R) (dashed); and cone tip-to-meniscus distance for the collapse of a conical bubble containing no gas (R_c) (dotted). The initial conditions are that $R = R_c = 52\,\text{mm}$; $\dot{R}_c = \dot{R} = 0$ and $h_i = 371\,\text{mm}$. The fixed apparatus dimensions are given in the text.

for the dimensions of the apparatus ($h \approx 400\,\text{mm}$, $r_{\max} = 52\,\text{mm}$), this implies the inertias are equal when $R_e \approx 6\,\text{mm}$. This is usually several times the radius the bubble had prior to expansion. Since $\Phi_{KE,c}$ decreases with increasing R_c (equation 6), but $\Phi_{KE,t}$ increases (since h increases with R_c, equations 7 and 8), it is clear that the inertia of the liquid in the tube dominates the early stages of a typical collapse. Control of h therefore enables control of the inertial forces at the start of the collapse. However in the final stages of the collapse, when it is desirable for the dynamic processes in the liquid surrounding the bubble to more closely resemble the collapse of a bubble in an unconstrained medium, with the appropriate pseudo-spherical liquid convergence and divergence, this is what the apparatus delivers.

Rayleigh's model of an inertial collapse of a spherical bubble will now be adapted for the conical case. The liquid velocity at the base of the cone, $\dot{\epsilon}$, is related to the bubble wall speed, $\dot{R}_c$, through $\dot{\epsilon}/\dot{R}_c = R_c^2/r_{\max}^2$ (by considering mass continuity, as in equation 5). Therefore balancing the work done by the application of a pressure step of magnitude p_∞, at the end of the column remote from the bubble, with the kinetic energy of the liquid (both in the tube and in the cone) gives a modified form of equation (1):

$$\begin{aligned}\frac{\pi}{3}p_\infty \tan^2\theta\left(R_i^3 - R_c^3\right) &= \Phi_{KE,c} + \Phi_{KE,t} \\ &= \frac{1}{2}\rho\pi \tan^2\theta\, r_{\max}^4 \left(\frac{\dot{R}_c R_c^2}{r_{\max}^2}\right)^2 \left(\frac{1}{R_c} - \frac{1}{r_{\max}}\right) \\ &+ \frac{1}{2}\rho\left(A_0 h_i - \frac{\pi}{3}\tan^2\theta\left(R_i^3 - R_c^3\right)\right)\left(\frac{\dot{R}_c R_c^2}{r_{\max}^2}\right)^2\end{aligned} \tag{10}$$

(explicitly substituting for the time dependent variable h using equation 8). The expression of the bubble wall speed, the conical equivalent to the spherical expression (equation 3) is:

$$\begin{aligned}\dot{R}_c^2 = \left(\frac{r_{\max}^2}{R_c^2}\right)^2 &\frac{\pi}{3}p_\infty \tan^2\theta\left(R_i^3 - R_c^3\right) \\ &\cdot\left\{\frac{1}{2}\rho A_0\left[\left(\frac{1}{R_c} - \frac{1}{r_{\max}}\right)r_{\max}^2 + h_i \right.\right. \\ &\left.\left. - \frac{1}{A_0}\frac{\pi}{3}\tan^2\theta\left(R_i^3 - R_c^3\right)\right]\right\}^{-1}.\end{aligned} \tag{11}$$

Equation (11) is plotted in Figure 3 and compared with the Rayleigh collapse of a spherical bubble (setting $R = R_c$ for comparative purposes). The initial bubble length R_i was taken to be the maximum meniscus displacement ($r_{\max}$) of 52 mm, and the tube contained an initial length of water h_i of 371 mm to mimic the experimental set-up. The value for A_0 is calculated as $2.8 \cdot 10^{-3}\,\text{m}^2$. The starting position ($\dot{R}_c = \dot{R} = 0$) cannot be shown on this logarithmic plot. However it is clear that in the early stages of the collapse the plots diverge (because of the contribution to the inertia of the liquid in the column). As the collapse proceeds (i.e. the vertical distance between tip and meniscus decreases), the two plots tend to converge (as the meniscus velocity increases).

The length of the liquid column in the tube required to most closely correspond with the spherical collapse (h_s) can be determined. This calculation is only an attempt to find approximately good solutions: the inertia of this experimental system can never exactly equal the inertia of the spherical one since the radiation mass of a fluid element depends critically on the geometry of the fluid flow, and for the portion of the fluid which enters the cone from the U-tube this geometry changes from parallel flow to converging flow. As such, the inertia of the liquid in the U-tube decreases during the collapse: since the discrepancy is greatest nearer the start, the bias in the balancing calculation to find h_s should be made for the situation nearer the early, rather than the later, stages of collapse. This is a sensible solution, since in the later stages the required length changes much more rapidly.

The parameter requiring balancing between the spherical and conical collapses is the radiation mass. This is defined for a spherical bubble of radius R in this "radius-force" frame [14] from consideration of the kinetic energy of the liquid, $\phi_{K,s}$ and the velocity of the bubble wall:

$$m_s = \frac{\phi_{K,s}}{\frac{1}{2}\dot{R}^2} = \frac{\int_R^\infty (4\pi r^2 \rho \mathrm{d}r)\dot{r}^2}{\frac{1}{2}\dot{R}^2} = 4\pi R^3 \rho \tag{12}$$

(evaluation of the integral being facilitated through use of equation 2). In the conical apparatus in question, the bubble fills the cone to R_c below the apex, giving the liquid in the cone an inertia of m_c. The required parameter is the length of fluid in the U-tube, h_s, with a particular inertia m_t, such that the total inertia of the liquid in the apparatus is the same as that for the spherical case. The ratio of the conical bubble volume to a spherical bubble of the same radius can be readily determined as $\tan^2\theta/4$, so calculating these radiation

ACUSTICA · acta acustica
Vol. 84 (1998)

inertias from the kinetic energies stated in equation (10), and letting $R = R_c$ for equivalence, gives

$$\begin{aligned} & \frac{\tan^2\theta}{4} m_s = m_c + m_t \\ \Rightarrow \quad & \frac{\tan^2\theta}{4} \frac{\phi_{K,s}}{\frac{1}{2}\dot{R}^2} = \frac{\Phi_{KE,c} + \Phi_{KE,t}}{\frac{1}{2}\dot{R}_c^2} \\ \Rightarrow \quad & \pi R_c^3 \rho \tan^2\theta = \\ & \rho A_0 \left(\frac{R_c}{r_{\max}}\right)^4 \left[\left(\frac{1}{R_c} - \frac{1}{r_{\max}}\right) r_{\max}^2 + h_s\right] \\ \Rightarrow \quad & h_s = r_{\max}. \end{aligned} \tag{13}$$

The liquid tube length of 40–45 cm used in these experiments is a compromise, giving more inertia than required during the collapse. A greater length would reduce the maximum size to which the bubble could grow prior to collapse (note that the measured pressures of around 700 Pa result almost entirely from the hydrostatic head), though the shape of the U-tube is designed to minimise this limitation (Figure 1a).

In his consideration of a spherical collapse, Rayleigh [1] went on to incorporate a permanent gas phase, such as is found in this experiment, within the bubble. He proposed that from an initial maximum radius R_m, when $\dot{R} = 0$, the cavity would collapse, and then rebound, and from thence oscillate between a maximum and a minimum value, $R = R_{\max}$ and $R = R_{\min}$ respectively, the wall speed being zero at the two extremes. In the absence of dissipation, clearly $R_{\max} = R_m$. Noltingk and Neppiras [3] completed the formulation.

It is possible to set out an analogous calculation for the collapse of the conical bubble. The meniscus is assumed to be a flat based segment at all times, and we define the pressure at the interface in the liquid to be p_L. When the top plate of the apparatus has been opened (Figure 1a), there is a step in this pressure at the bubble wall, and from this time the value for p_L would be $p_\infty + \rho g \Delta h$, where Δh is the dynamic difference in height between the meniscus and the water level in the open tube. The apparatus is designed in such a way, however, that the water fills two legs of a U-tube to roughly the same height, and therefore this height difference is always less than 10 cm. This dynamic contribution to the value of p_L is $< 1\%$ of the static value, and can therefore be neglected.

The energy balance before and after the start of the collapse can now be considered. The increase of kinetic energy of the liquid in the tube and cone must be equal to the work done by the gas at the interface as the radius changes from R_i to R_c. Due to the presence of gas inside the bubble, the second term requires a knowledge of the pressures on both sides of the meniscus, and hence an expression for the internal gas pressure p_g. At the start of the collapse, when $R_c = R_i$ and $\dot{R}_c = 0$, the gas within the bubble has pressure $p_{g,i}$ and temperature T_i. If there is no heat flow across the bubble wall (which is valid if the collapse speed is fast), the gas pressure p_g and bubble volume follow an adiabatic relationship. If the vapour pressure is assumed to be negligible, equating the initial conditions with those of a general meniscus position

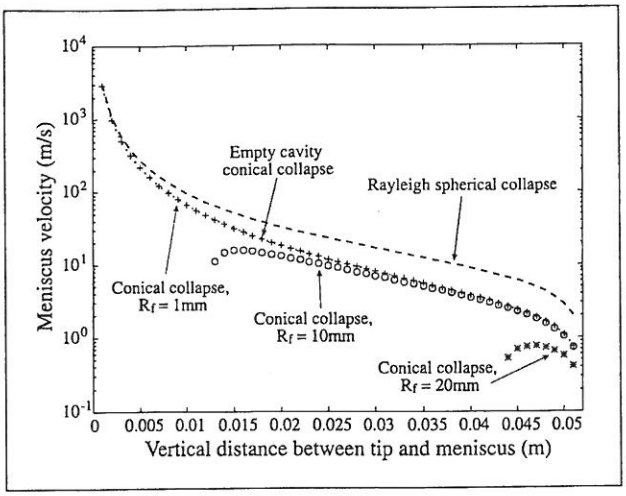

Figure 4. Plot of meniscus velocity against bubble radius for the two empty cavity cases shown in Figure 3, plus the meniscus velocity of the collapse of gas filled bubbles of final spherical radii 1 mm (+), 10 mm (o) and 20 mm (*). The initial conditions are as described in Figure 3.

gives:

$$\begin{aligned} & p_{g,i}\left(\frac{\pi}{3} R_i^3 \tan^2\theta\right)^\gamma = p_g \left(\frac{\pi}{3} R_c^3 \tan^2\theta\right)^\gamma \\ \Rightarrow \quad & p_g = p_{g,i} \left(\frac{R_i}{R_c}\right)^{3\gamma}. \end{aligned} \tag{14}$$

Therefore the work done by the gas in the bubble on the liquid interface can be written as:

$$\begin{aligned} WD &= \int_{R_i}^{R_c} (p_g - p_L)\pi (R_c' \tan\theta)^2 \, \mathrm{d}R_c' \\ &= \int_{R_i}^{R_c} \left(p_{g,i}\left(\frac{R_i}{R_c'}\right)^{3\gamma} - p_L\right) \pi (R_c' \tan\theta)^2 \, \mathrm{d}R_c' \\ &= \frac{\pi \tan^2\theta}{3} \Bigg[p_L (R_i^3 - R_c^3) \\ &\qquad + \frac{p_{g,i} R_i^{3\gamma}}{(\gamma - 1)} \left(R_i^{3(1-\gamma)} - R_c^{3(1-\gamma)}\right) \Bigg], \end{aligned} \tag{15}$$

where R_c' has been used as the integration variable. Using the kinetic energy terms derived earlier, the total kinetic energy of the liquid can be equated with the work done thus:

$$\begin{aligned} & \frac{\pi \tan^2\theta}{3} \Bigg[p_L (R_i^3 - R_c^3) \\ & \quad + \frac{p_{g,i} R_i^{3\gamma}}{(\gamma - 1)} \left(R_i^{3(1-\gamma)} - R_c^{3(1-\gamma)}\right) \Bigg] \\ = \; & \frac{1}{2} \rho \pi \tan^2\theta \, r_{\max}^4 \dot{\varepsilon}^2 \\ & \cdot \left(\frac{1}{R_c} - \frac{1}{r_{\max}}\right) + \frac{1}{2} A_0 \rho h \dot{\varepsilon}^2. \end{aligned} \tag{16}$$

Using the substitution for h defined in equation (8) and replacing $\dot{\varepsilon}$ using the continuity relationship as before, gives

an expression for the speed of the bubble wall as:

$$\dot{R}_c^2 = \left(\frac{r_{\max}}{R_c}\right)^4 \frac{\pi \tan^2\theta}{3}\left[p_L(R_i^3 - R_c^3) - \frac{p_{g,i}R_i^3}{(\gamma-1)}\left(\left(\frac{R_i}{R_c}\right)^{3(\gamma-1)} - 1\right)\right] \cdot \left\{\frac{1}{2}\rho A_0\left[\left(\frac{1}{R_c} - \frac{1}{r_{\max}}\right)r_{\max}^2 + h_i - \frac{1}{A_0}\frac{\pi}{3}\tan^2\theta(R_i^3 - R_c^3)\right]\right\}^{-1}. \quad (17)$$

Therefore if $p_{g,i}$ is set to zero, and the gas content of the bubble is effectively removed, equation (17) becomes equation (11) from earlier. This is shown in Figure 4, for the same experimental conditions as those used in Figure 3. The plot shows the meniscus velocity for the two empty cavity conditions described earlier, as well as those corresponding to gas inclusions in the cone tip whose final radii (R_f) were 1 mm, 10 mm and 20 mm. These final bubble radii are not the same as the equivalent conical radii, as used throughout this paper; but rather radii of spherical bubbles, as it was observed experimentally that the final inclusions adopted a spherical form which sat at the tip of the cone. Whilst bubbles of the size ($R_f \approx 1$ mm) typically used in the experimental investigation closely follow the empty cavity collapse, the collapse of bubbles with larger R_f is cushioned significantly by the gas.

As described earlier, the conical bubble starts the collapse with a zero wall velocity and a maximum radius R_i, with the gas within the bubble having pressure $p_{g,i}$ and temperature T_i. The wall velocity will next be zero at the minimum radius $R_{\min}$, when the pressure and temperature of the gas within the bubble are at a maximum, $p_{g,\max}$ and $T_{\max}$ respectively. Assuming no break-up, the bubble will then rebound to reach a maximum size of $R_{\max}$, which if no losses are included will also equal R_i. The positions of maximum and minimum radius are found by setting $\dot{R}_c = 0$ in equation (17), such that

$$\left[p_L(R_i^3 - R_c^3) - \frac{p_{g,i}R_i^3}{(\gamma-1)}\left(\left(\frac{R_i}{R_c}\right)^{3(\gamma-1)} - 1\right)\right] = 0, \quad (R_c = R_{\max}, R_{\min}). \quad (18)$$

As expected, one solution to equation (18) gives the position of $R_{\max} = R_i$, the initial radius. The other solution occurs at $R_c = R_{\min}$. Simple estimates in the limit of $R_{\min} \ll R_i$ can be made by simplifying equation (18), to give:

$$R_{\min} = R_i\left[\left(\frac{p_{g,i}}{p_L(\gamma-1)}\right)\right]^{\frac{1}{3(\gamma-1)}}. \quad (19)$$

The only value which is unknown in this expression is $p_{g,i}$ the initial bubble gas pressure. This can be estimated from the final, post-collapse conditions, as follows (provided mass loss or gain from the bubble is negligible). As described above, after the plate has been released and all the energy has been dissipated from the collapse, experimental observations have shown a spherical bubble lying at rest just below the tip of the cone. The difference in state between this bubble and the initial (before plate opening) bubble are governed by an isothermal relationship in volume and pressure, as both states will be at the initial temperature T_i. As such:

$$p_{g,i}\frac{\pi}{3}R_i^3\tan^2\vartheta = p_L\frac{4}{3}\pi R_f^3$$

$$\Rightarrow \quad p_{g,i} = \frac{4}{\tan^2\vartheta}\left(\frac{R_f}{R_i}\right)^3 p_L, \quad (20)$$

where R_f is the spherical radius of the final bubble in the cone tip. It is assumed that the static liquid pressure on the bubble prior to growth, equals the pressure step p_L which collapses the bubble. Equation (20) again ignores the contribution to the internal pressure of the bubble due to the difference in height of the liquid in the two legs of the U-tube, and also any contribution due to the Laplace pressure (which for a $1mm$ radius bubble, will be $\sim 0.1\%$ of the static pressure contribution). A more complete but mathematically exhaustive form of the theory has been performed which includes the height difference, but the results show that there is a negligible change in the collapse conditions from the approximate version considered here.

However, although the estimate for $R_{\min}$ calculated from the assumption that $R_{\min} \ll R_i$ described in equation (19) is valid for large initial meniscal displacements, a more exact solution is available through calculation of $R_{\min}$ iteratively using Newton-Raphson's method. This divergence is illustrated in Figure 5 for a bubble of final radius 6 mm, where it can be seen that as the initial bubble size becomes smaller, the estimate in equation (19) produces higher values for $R_{\min}$ than would be expected. This becomes important in calculating the maximum tip pressures in the bubble later on, although for large bubbles the approximation is valid. The maximum pressure achieved in the collapse, at a time when $R_c = R_{\min}$, can be found by assuming the collapse to be

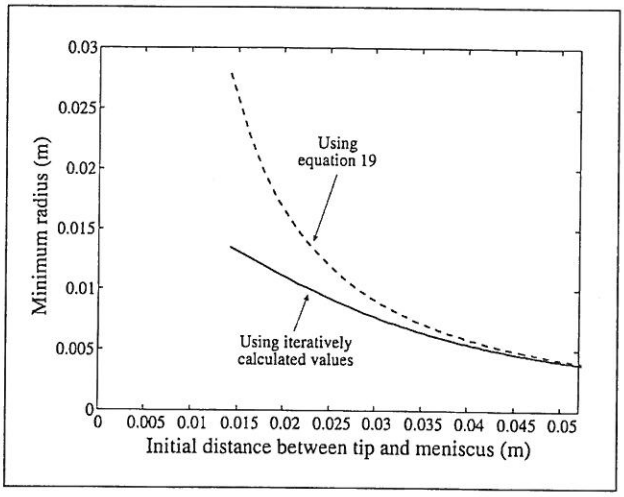

Figure 5. Calculation of the minimum radius attained by a 6 mm final radius bubble calculated using the approximation in equation (19) (dashed), and using an exact expression calculated iteratively (unbroken).

ACUSTICA · acta acustica
Vol. 84 (1998)

adiabatic, and replacing the expression for $p_{g,i}$ derived in equation (20):

$$p_{g,\max} = p_{g,i}\left(\frac{R_i}{R_{\min}}\right)^{3\gamma} = \left[\frac{4}{\tan^2\vartheta}\left(\frac{R_f}{R_i}\right)^3\right]^{\frac{1}{1-\gamma}}\left[\gamma-1\right]^{\frac{\gamma}{\gamma-1}} p_L \tag{21}$$

and, following the same reasoning, the maximum temperature reached in the bubble can be expressed as:

$$T_{\max} = T_i\left(\frac{R_i}{R_{\min}}\right)^{3(\gamma-1)} = \left[\frac{4}{\tan^2\vartheta}\left(\frac{R_f}{R_i}\right)^3\right]^{-1}(\gamma-1)T_i. \tag{22}$$

Several workers have adapted the Noltingk-Neppiras model to estimate the likely pressures and temperatures attained during an inertial collapse, for such purposes as defining and investigating the threshold conditions (in acoustic pressure amplitude, temporal characteristics of sinusoidal or Gaussian pressure waves, etc.) required to bring about inertial cavitation [24, 25, 26, 27, 28]. In many cases it is assumed that the bubble reached the conditions for the start of the collapse following an initial isothermal growth phase [29] from a seed nucleus. In all other experimental situations to date it has not been possible to separate out the collapse from the growth phase. With the conical bubble, the slow isothermal growth is practical, the facility being there to hold the bubble at maximum size indefinitely. The experiment therefore eliminates the uncertainty of the growth phase, and allows the conditions at the start of the collapse (usually not amenable to ready measurement) to be measured accurately. Previously for example, even the maximum radius prior to collapse has had to be estimated [5, 6, 28, 29, 30]. In addition, the current apparatus allows sensors to be placed in the liquid close to the bubble wall, and, to a certain extent, within the bubble itself.

2. Apparatus

The basic apparatus consists of a steel U-tube, of 60 mm internal diameter, partially filled with degassed water (Figure 1). The internal pressure within the tube can be reduced through connections to a vacuum pump above the level of the liquid in the longer leg of the tube, which is terminated by a spring-loaded plate [31]. Once the valve to the vacuum pump is closed, the raising of this plate using the lever returns the pressure exerted on the tube contents to atmospheric. The shorter leg is terminated by a transparent hollow cone of 30° half-angle. When under atmospheric pressure, this leg and cone are filled with water, except for a bubble of milllimetre-order diameter which is injected into the apex of the cone down a length of rubber tubing which is temporarily fed through the length of the U-tube. When the pressure in the U-tube is reduced, this bubble grows, to violently collapse into the apex of the cone when the plate is raised. This collapse could generate sonoluminescence.

The cone being transparent (45 ±5% of photons produced at the tip reaching the cone exterior), various optical instruments could be deployed to study the collapse, though not simultaneously, including video photography at 50 frames per second (f.p.s.) using a Hadland Photonics HSV and two synchronised stroboscopes, of 20 μs flash duration. Operating at 25 f.p.s., a CCD camera (Photonic Science DS 800) imaged not only the cone (weakly-illuminated from behind by a flat beta light produced by painting phosphorous over a tritium source), but also the sonoluminescence. The CCD camera system produces each frame by interlacing two fields, each of 40 ms duration, each being 20 ms out of phase with the other. Therefore, in keeping with the 25 f.p.s. video recording, there is a frame every 40 ms, but in every such frame there is some information gathered over 60 ms. Each field integrates the light for only 18.4 ms (the remaining 1.6 ms being taken up by blanking filters). The persistence on the intensifier system is less than 3 ms for the exposures used, and so will not affect the images presented here. Both cameras (HSV and DS 800) were connected to a video recorder (Panasonic NV-FS 88 HQ) using S-VHS videotape.

Time-resolution and limited quantification of the sonoluminescence could be made using a photomultiplier tube (EMI 9893B/30) supplied with 1640 V (Brandburg 475R power supply), giving a dark count of $9\,s^{-1}$. The voltage signal for the LeCroy 9314L oscilloscope, with a sampling rate of 100 MHz, was provided across the variable resistor (10 Ω–100 kΩ). A single photon would therefore produce a trace resembling an exponentially-decaying oscillation at frequency $1/(2\pi\sqrt{LC}) = 43$ MHz, where $L = 89$ nH is the inductance, and $C = 149$ pF the capacitance, of the system. An optimal resistance of 300 Ω compromised adequately in control of signal amplitude and decay time.

None of the optical instruments described above could be deployed simultaneously because of their differing ambient light requirements. However instrumentation to measure the pressure, and indicate the level, of the liquid could be deployed simultaneously with them. These instruments are mounted in the 62 mm tall polymethylmethacrylate (PMMA) extension to the shorter leg of the U-tube (Figure 1a). Within this extension, a pressure transducer (RS341-979), the centre of its 5.1 mm diameter placed 5 cm below the start of the cone, recorded the pressure fluctuations within the liquid close to the bubble. Such fluctuations measured by this 'liquid pressure transducer (LPT)' include: the pressure reduction before release of the plate (cross-checked with a pressure gauge fitted to the pumping train); the pressure wave which propagates through the U-tube in response to the opening of the plate; and the rebound pressure pulses emitted by the bubble (the latter sometimes being of a magnitude beyond the linear range of the LPT (0–0.21 MPa), outside of which no calibration could be obtained from the manufacturers). The extension was removed when rebound pressures great enough to permanently affect its performance were planned. The characteristic response time of the LPT is 0.5 ms, indicating the limits of its temporal resolution.

The apex of the cone was designed to itself take inserts (shown in Figure 1), of 47 mm length and 25 mm outer diameter, containing a 30° half-angle conical space which, at its 13 mm diameter base, is commensurate with the aperture caused by the truncation of the main cone. The stresses at the cone tip resulting from the bubble collapse, be they gas pressures or the result of jets, are sufficient to damage PMMA cone tips. Such is to be avoided, if only to remove the possibility that a contribution to the luminescence might otherwise be triboluminescent in origin. Therefore for collapses capable of damaging PMMA cone tips, such as those reported in this study, polycarbonate cone tip inserts were used, which though tougher are less transparent. Though the apparatus could still generate collapses capable of cracking polycarbonate, the results presented in this paper did not do so. Though conical inserts were used in all measurements of sonoluminescence, a second type of insert could be employed (Figure 1b). This insert truncates the cone 5.25 mm before the apex by placing there a transducer (Keller PA-8, termed here High Pressure Transducer, HPT, and having 30 kHz resonance) which the manufacturers calibrate up to 1000 bar: However here only the central circular area (6.05 mm diameter) of the full 13.0 mm diameter face of the transducer is exposed.

3. Results

Figure 6 shows the CCD records of sonoluminescence from a range of collapses. In these figures, the cylindrical insert is clearly visible: its dark edges (spaced 25.1 mm apart, the diameter of the insert) are clearly visible, arrowed in Figure 6b frame 1. Midway between these arrows the tip of the cone, hollowed out of this insert, is visible as a dark region, as it scatters the back-lighting away from the camera. Sonoluminescence is recognised as bright light sources within the cone, which appear on the video recording at the same time as the explosive sound that follows the release of the vacuum. Care must be taken in interpretation of such images. First, genuine sonoluminescence will have the same temporal characteristics as will its reflection in PMMA surfaces. Second, persistence of sufficiently bright sources on intensified images may be longer than the interframe time, making it impossible to distinguish between persistence in the luminescence and persistence in the camera system. Third, the presence of two regions of luminescence in one frame does not imply that they occurred simultaneously, only that emission (or persistence) occurred from both regions within the frame exposure. All measurements from Figure 6 are ±0.5 mm.

The luminescence generally appears in three regions. Firstly (and most commonly) it fills the cone from the apex to a distance of some 2 mm below it, as shown in Figure 6a. The second region is shown in Figure 6b. The system detects no luminescence at the cone tip, but rather in an elliptical region some 4 mm×2 mm, its centre being about 6 mm below the tip. The region is not symmetrical about the axis of the cone, but when it appeared in this form the location

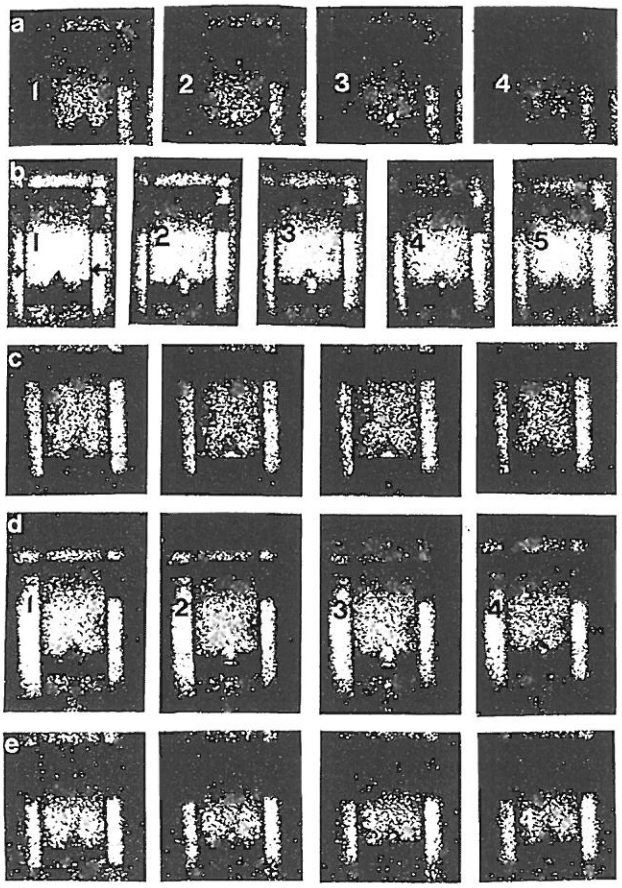

Figure 6. Sonoluminescence imaged in the cone tip (interframe time = 40 ms, but each frame is interlaced as detailed in the text). Weak back-lighting is provided so that the tip of the cone is shown in silhouette. (a) Luminescence is seen only at the tip. Pre-collapse (i.e. fully-expanded) bubble volume was 177 ml. The volume of water in the device was 1100 ml, and initial (pre-growth) bubble volume was 0.065 ml. (b) Luminescence appears as an off-axis ellipse with slight fringe below. Pre-collapse (i.e. fully-expanded) bubble volume was 154 ml. The volume of water in the device was 1100 ml, and initial bubble volume was 0.065 ml. The boundaries of the insert, 25.1 mm apart, are arrowed in frame 1. (c) A fringe of luminescence occurs at the base of the insert. Pre-collapse (i.e. fully-expanded) bubble volume was 28 ml. The volume of water in the device was 1100 ml, and initial bubble volume was 0.76 ml. (d) Luminescence occurs at several sites (at cone tip as in (a), as an ellipse as in (b), and thirdly a fringe as in (c)). Pre-collapse bubble size was 77 ml, and initial bubble size was 0.065 ml. The volume of water in the device was 1100 ml. (e) One small bright spot of luminescence occurs on the axis of the insert, approximately 5 mm below cone tip. Pre-collapse (i.e. fully-expanded) bubble volume was 49 ml. The volume of water in the device was 1100 ml, and initial bubble volume was 0.76 ml.

was asymmetric in the same direction (i.e. to the right in this picture). This suggests that the source of the asymmetry, which defines the direction of the anisotropy, lies in the apparatus itself. The third region comprises a line some 8 mm below the cone apex (Figure 6c). The base of the insert occurs in this region, raising the possibility that this might be sonoluminescence, or that luminescence generated below the frame is scattered from the PMMA. Figure 6d does show luminescence from the three regions mentioned above during the same collapse. However the 'line' appears more well-defined, and occurs only directly below other luminescing

ACUSTICA · acta acustica
Vol. 84 (1998)

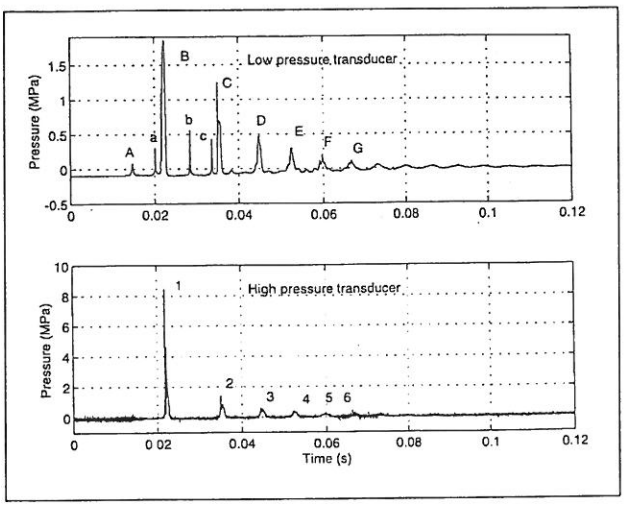

Figure 7. Pressure traces recorded simultaneously by pressure transducers LPT (in the tube) and HPT (at the tip) showing rebound pressure pulses (labelled '1', '2', etc. and 'B', 'C', etc.) and reflections of these pulses within the apparatus.

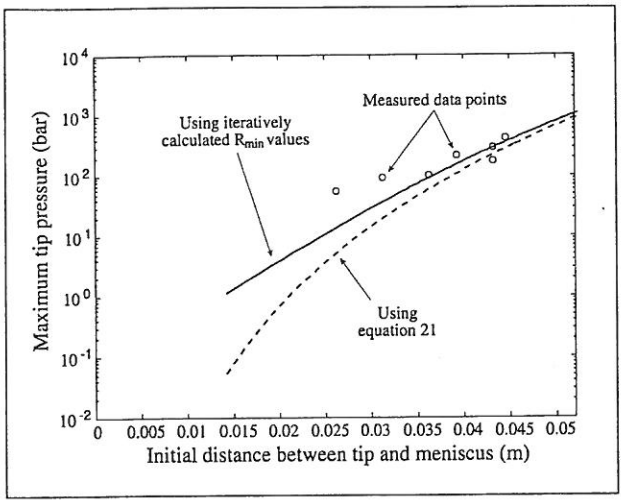

Figure 8. Maximum pressure amplitudes reached at the cone tip as measured by HPT (equivalent to '1' in Figure 5 but scaled appropriately) compared to both equation 21, which uses an estimate for $R_{\min}$, and a solution using $R_{\min}$ obtained iteratively using the Newton-Raphson method.

regions which may provide light for scattering, in a manner similar to 6b. Therefore in Figures 6b and 6d the detection of light from the 'line' region may well result from scattering, and cannot be categorically taken to indicate sonoluminescence from the line. During one collapse luminescence was imaged from none of the above locations, but instead from only a relatively concentrated location some 3 mm below the cone appex (Figure 6e).

Figure 7 shows the pressure traces recorded by the LPT and HPT simultaneously. The HPT trace enables ready identification of the times when the gas pressure is greatest, labelled '1' (initial collapse), '2' etc. The corresponding pressure pulses emitted into the liquid on rebound are detected shortly afterwards (the interval being the propagation time) in the LPT trace ('B', 'C', 'D', 'E', 'F', 'G'). The passage over the LPT of the initial shock wave which follows from the opening of the plate is labelled 'A'. The other peaks ('a', 'b', 'c') correspond to reflections of the above already-mentioned pulses within the apparatus [32].

Figure 8 shows the maximum amplitudes of the HPT trace corresponding to the first collapse (i.e. equivalent to '1' in Figure 7) for different pre-collapse bubble sizes. Transducer pressures are indicated on the left axis. A bubble of initial volume 0.9 ml under atmospheric pressure grows to a pre-collapse size as given on the horizontal axis under a partial vacuum. The manufacturer's calibration for the HPT was used, which assumes an even pressure is applied over the face of the transducer. However as described earlier, only a 6 mm diameter central region of the bubble was exposed by the PMMA insert.

The transducer manufacturer was unable to assist in estimation of the true pressures if the face is only partially exposed. In the absence of such guidance, if it is assumed that a partially-exposed face underestimates the pressure by the proportion of coverage, this would suggest that the true pressure at the truncated cone apex is $(13.0/6.05)^2 = 4.6$ times the value given in Figure 7, more so when the high pressure region on the transducer covers less than the 6 mm diameter exposed face (for example, if the bubble contracts to less then 3 mm radius, or involutes to form a jet smaller than this). The total volume of liquid in the apparatus was 1050 ml. Plotted also on the figure are the predictions for the maximum gas pressure attained during the collapse. Two curves are plotted: one is calculated from equation (21) and uses equation (19) as an approximation for $R_{\min}$, the other uses values of $R_{\min}$ calculated iteratively using the Newton-Raphson method.

Other information contained within the LPT trace comes through the evidence of repeated collapses and rebounds. The high speed video evidence clearly shows fragmentation within the first 20 ms of the first rebound [32]. However the pressure transducer always shows repeated rebounds for at least 80 ms after the initial rebound. The conclusion is that, whilst the meniscus does become unstable, some coherent action of gas bodies occurs at the apex: either the bubble fragments on rebound but then coalesces as the cloud of fragments are forced together in a subsequent collapse; or the pressure pulses detected on the HPT and LPT result from some co-operative pulsation of the fragments; or the whole bubble does not fragment uniformly, but instead produces a large number of smaller bubbles whilst retaining the single original bubble otherwise intact.

Figure 9 shows the variation, as a function of the liquid volume within the apparatus, of the number of discernible arrivals in the sonoluminescent burst associated with the first rebound emission. Counts for liquid volumes of 1150 ml or less represent lower estimates only, as the record from the photomultiplier contained regions within each burst where arrivals occurred more closely than the resolution limit of 50 ns. For such intervals the lower limit of the count was estimated by assuming one arrival per 50 ns interval. The liquid pressure at the first rebound is shown. For each liq-

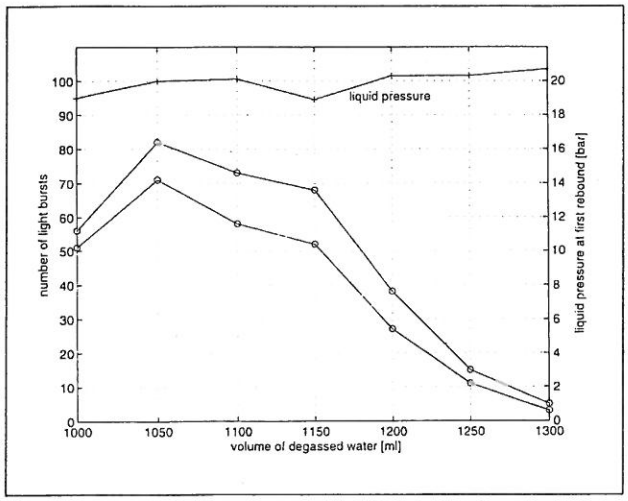

Figure 9. The variation, as a function of the liquid volume, of the number of discernible arrivals in the sonoluminescent burst associated with the first rebound emission. The liquid pressure at the first rebound is also shown. Dark count: $9\,s^{-1}$. Photocathode conversion efficiency: 20%. Proportion of photons not absorbed by polycarbonate and PMMA: 44%. The overall photon collection efficiency of the system, given the 9 mm diameter photocathode placed 24 cm from the cone tip subtends a solid angle of 0.0011 steradian, is therefore $(0.0011/4\pi) \times 0.44 \times 0.2 \times 100\% \approx 0.0008\%$.

uid volume, two experiments were performed. Although the aliasing described above should be recalled, Figure 9 can be compared with the results of Chendke and Fogler [33], who measured the amount of sonoluminescence from multi-bubble ultrasonic cavitation as a function of varying hydrostatic pressure. They found that whilst high static pressures tended to suppress bubble growth, a smaller increase in static pressure would increase the sonoluminescence by enhancing the collapse phase of the bubble. In the present experiment there is, in addition to these two effects, the change to the inertia associated with the collapse which varying amounts of liquid will produce.

4. Discussion and conclusions

It must be emphasised at the outset of this discussion that the bubble collapse studied here is not identical to the collapse of a segment of a spherical bubble. When the radius (the distance from the cone apex to the meniscus) is large, most of the bubble wall (that is, apart from the region where it meets the PMMA) is planar and, as discussed in the Introduction, the question of the stability of a planar interface is quite different from that of a spherical one. Unless instabilities generated at an earlier stage have become pronounced at the later stages, then the spherical approximation may be good when the bubble volume is small. The key points are that this system does produce sonoluminescence; involves an unstable bubble collapse whereby the production of a large number of small bubble fragments at the interface nevertheless leaves a bubble relatively intact at the end; and involves two distinct classes of feature. In quantity and timing, both the sonoluminescence commensurate with the initial collapse, and the pressure waves emitted into the liquid by rebound of the main bubble, are repeatable (within the limits of replication of initial parameters of the collapse). As such, and in line with current theory, these features are taken to have their origin in the dynamics of the mother bubble.

Though interesting, the question remains as to what use the experimental system described in this paper might have to research in bubble collapse. The collapse generates sonoluminescence, but the experiments reported here at the moment support no one mechanism for its production over another. The agreement between the measured collapse pressures and those predicted by the adiabatic theory is surprising, since such theory is perhaps the simplest description of a bubble collapse capable of generating sonoluminescence. The pressures exerted on the sensor are likely to require theories incorporating inhomogeneous pressure distributions within the gas, distortions of the bubble wall, or liquid impact for a full description. Nevertheless at the foundation of the widely-adopted mechanical index [27, 28, 34] is a similar calculation, relating to the temperature attained by the gas; and underlying all of these are the pioneering calculations of Rayleigh, Neppiras and Noltingk, which decades on still have current application.

Acknowledgement

The authors are very grateful to Mr. Ray Flaxman for his excellent technical assistance and insights in the construction of the U-tube apparatus, and to Dave Johnson for his contribution.

References

[1] Lord Rayleigh: On the pressure developed in a liquid during the collapse of a spherical cavity. Phil. Mag. **34** (1917) 94–98.
[2] F. G. Blake: Technical Memo No.12. Acoustics Research Laboratory, Harvard University, Cambridge, Massachusetts, USA, 1949.
[3] B. E. Noltingk, E. A. Neppiras: Cavitation produced by ultrasonics. Proc. Phys. Soc., B **63** (1950) 674–685.
[4] E. A. Neppiras, B. E. Noltingk: Cavitation produced by ultrasonics: Theoretical conditions for the onset of cavitation. Proc. Phys. Soc., B **64** (1951) 1032–1038.
[5] H. G. Flynn: Physics of acoustic cavitation in liquids. – In: Physical Acoustics. W. P. Mason (ed.). Academic Press, New York, 1964, 57–172.
[6] H. G. Flynn: Cavitation dynamics. II. Free pulsations and models for cavitation bubbles. J. Acoust. Soc. Am. **58** (1975) 1160–1170.
[7] R. A. Roy, A. A. Atchley, L. A. Crum, J. B. Fowlkes, J. J. Reidy: A precise technique for the measurement of acoustic cavitation thresholds and some preliminary results. J. Acoust. Soc. Am. **78** (1985) 1799–1805.
[8] R. E. Apfel: Acoustic cavitation prediction. J. Acoust. Soc. Am. **69** (1981) 1624–1633.
[9] D. F. Gaitan, L. A. Crum: Observation of sonoluminescence from a single cavitation bubble in a water/glycerine mixture. – In: Frontiers of Nonlinear Acoustics, 12th ISNA. M. F. Hamilton, D. T. Blackstock (eds.). Elsevier, New York, 1990, 459.
[10] T. G. Leighton: Bubble population phenomena in acoustic cavitation. Ultrasonics Sonochemistry **2** (1995) 123–136.

[11] T. H. Matula, R. A. Roy, W. B. Mourad, W. B. McNamara, K. S. Suslick: Comparison of multi-bubble and single-bubble sonoluminescence. Phys. Rev. Lett. **75** (1995) 2602–2605.
[12] T. J. Matula, R. A. Roy, P. D. Mourad: Optical pulse width measurements of sonoluminescence in cavitation-bubble fields. J. Acoust. Soc. Am. **101** (1997) 1994–2002.
[13] T. J. Matula, R. A. Roy: Comparisons of sonoluminescence from single bubbles and cavitation fields: bridging the gap. Ultrasonics Sonochemistry **1997** (in press).
[14] T. G. Leighton: The acoustic bubble. Academic Press, London, 1994.
[15] B. P. Barber, R. Hiller, K. Arisaka, H. Fetterman, S. Putterman: Resolving the picosecond characteristics of synchronous sonoluminescence. J. Acoust. Soc. Am. **91** (1992) 3061–3063.
[16] L. A. Crum, S. Putterman: Sonoluminescence. J. Acoust. Soc. Am. **91** (1992) 517.
[17] W. C. Moss, D. B. Clarke, W. White, D. A. Young: Hydrodynamic simulations of bubble collapse and picosecond sonoluminescence. Phys. Fluids **6** (1994) 2979–2985.
[18] C. C. Wu, P. H. Roberts: Shock-wave propagation in a sonoluminescing gas bubble. Phys. Rev. Lett. **70** (1993) 3424–3427.
[19] L. A. Crum, S. Cordry: Single-bubble sonoluminescence. – In: Bubble Dynamics and Interface Phenomena (Proc. IUTAM Symposium Birmingham, UK, 6-9 September 1993). J. R. Blake, J. M. Boulton-Stone, N. H. Thomas (eds.). Kluwer Academic Publishers, 1994, 287–297.
[20] T. Lepoint, N. Voglet, L. Faille, F. Mullie: Bubbles deformation and interface distortion as a source of sonochemical and sonoluminescent activity. – In: Bubble Dynamics and Interface Phenomena, (Proc. IUTAM Symposium, Birmingham, UK, 6-9 September 1993). J. R. Blake, J. M. Boulton-Stone, N. H. Thomas (eds.). Kluwer Academic Publishers, 1994, 321–333.
[21] C. Eberlein: Sonoluminescence as quantum vacuum radiation. Physics Review Letters, **76** (1996) 3842.
[22] A. P. Prosperetti: A new mechanism for sonoluminescence. J. Acoust. Soc. Am. **101** (1997) 2003–2007.
[23] Besant: Hydrostatics and hydrodynamics. CUP, London, 1859, §158.
[24] J. Sponer: Dependence of ultrasonic cavitation threshold on the ultrasonic frequency. Czech J. Phys., B **40** (1990) 1123–1132.
[25] J. Sponer, C. Davadorzh, V. Mornstein: The influence of viscosity on ultrasonic cavitation threshold for sonoluminescence at low megahertz region. Studia Biohys **137** (1990) 81–89.
[26] J. Sponer: Theoretical estimation of the cavitation threshold for very short pulses of ultrasound. Ultrasonics **29** (1991) 376–380.
[27] C. K. Holland, R. E. Apfel: An improved theory for the prediction of microcavitation thresholds. IEEE Transactions on Ultrasonics, Ferroelectrics, and Frequency Control **36** (1989) 204–208.
[28] R. E. Apfel, C. K. Holland: Gauging the likelihood of cavitation from short-pulse, low-duty cycle diagnostic ultrasound. Ultrasound in Med. and Biol. **17** (1991) 179–185.
[29] R. E. Apfel: Possibility of microcavitation from diagnostic ultrasound. IEEE Trans. Ultrason. Ferroelec. Freq. Contr. vol. **UFFC-32** (1986) 139–142.
[30] A. J. Walton, G. T. Reynolds: Sonoluminescence. Advances in Physics **33** (1984) 595–660.
[31] P. G. Kosky, G. A. Henwood: A new technique for investigating vapour bubble implosion experimentally. Brit. J. Appl. Phys. (J. Phys. D) Ser. 2 **2** (1969) 630–634.
[32] T. G. Leighton, W.-L. Ho, R. Flaxman: Sonoluminescence from the unstable collapse of a conical bubble. Ultrasonics **35** (1997) 399–405.
[33] P. K. Chendke, H. S. Fogler: Variation of sonoluminescence intensity of water with the liquid temperature. J. Phys. Chem. **89** (1985) 1673–1677.
[34] American Institute of Ultrasound in Medicine (AIUM): Standards for real-time display of thermal and mechanical acoustic indices on diagnostic ultrasound equipment. Laurel, MN, AIUM, 1992.